High-energy breakup of ^{6}Li as a tool to study the Big Bang nucleosynthesis reaction ^{2}H(α,γ)^{6}Li

F. Hammache,[1,2] M. Heil,[2] S. Typel,[2,3] D. Galaviz,[4,*] K. Sümmerer,[2,†] A. Coc,[5] F. Uhlig,[2] F. Attallah,[2] M. Caamano,[6] D. Cortina,[6] H. Geissel,[2] M. Hellström,[2] N. Iwasa,[7] J. Kiener,[5] P. Koczon,[2] B. Kohlmeyer,[8] P. Mohr,[4,‡] E. Schwab,[2] K. Schwarz,[2] F. Schümann,[9] P. Senger,[2] O. Sorlin,[1,§] V. Tatischeff,[5] J. P. Thibaud,[5] E. Vangioni,[10] A. Wagner,[11] and W. Walus[12]

[1]*Institut de Physique Nucléaire, UMR-8608, CNRS/IN2P3 and Université Paris Sud XI, F-91406 Orsay, France*

[2]*GSI Helmholtzzentrum für Schwerionenforschung GmbH, D-64220 Darmstadt, Germany*

[3]*Excellence Cluster "Origin and Structure of the Universe", Technische Universität München, D-85748 Garching, Germany*

[4]*Technische Universität Darmstadt, D-64220 Darmstadt, Germany*

[5]*Centre de Spectrométrie Nucléaire et de Spectrométrie de Masse (CSNSM), UMR-8609, CNRS/IN2P3 and Université Paris Sud XI, F-91405 Orsay Campus, France*

[6]*Universidade Santiago de Compostela, E-15786 Santiago, Spain*

[7]*Tohoku University, Aoba, Sendai, Miyagi 980-8578, Japan*

[8]*Fachbereich Physik, Philipps Universität, D-35032 Marburg, Germany*

[9]*Ruhr-Universität Bochum, D-44780 Bochum, Germany*

[10]*Institut d'Astrophysique de Paris, UMR-7095, CNRS and Université Pierre et Marie Curie, F-75014 Paris, France*

[11]*Forschungszentrum Rossendorf, D-01314 Dresden, Germany*

[12]*Institute of Physics, Jagiellonian University, PL-30-059 Krakow, Poland*

(Received 30 July 2010; revised manuscript received 29 November 2010; published 27 December 2010)

The recently claimed observations of non-negligible amounts of ^{6}Li in old halo stars have renewed interest in the Big Bang nucleosynthesis (BBN) of ^{6}Li. One important ingredient in the predicted BBN abundance of ^{6}Li is the low-energy ^{2}H(α,γ)^{6}Li cross section. Up to now, the only available experimental result for this cross section showed an almost constant astrophysical S factor below 400 keV, contrary to theoretical expectations. We report on a new measurement of the ^{2}H(α,γ)^{6}Li reaction using the breakup of ^{6}Li at 150 A MeV. Even though we cannot separate experimentally the Coulomb contribution from the nuclear one, we find clear evidence for Coulomb-nuclear interference by analyzing the scattering angular distributions. This is in line with our theoretical description, which indicates a drop of the S_{24} factor at low energies as predicted also by most other models. Consequently, we find even lower upper limits for the calculated primordial ^{6}Li abundance than before.

DOI: 10.1103/PhysRevC.82.065803 PACS number(s): 25.40.Lw, 25.60.Gc, 25.70.De, 26.35.+c

I. INTRODUCTION

The Big Bang model of the Universe is mainly supported by three pieces of observational evidence: the expansion of the Universe, the cosmic microwave background (CMB), and the primordial or Big Bang nucleosynthesis (BBN) of light nuclei like ^{2}H, ^{3,4}He, and ^{7}Li with one free parameter, the baryonic density of the Universe, Ω_b. Recently, a precise value for this free parameter ($\Omega_b h^2 = 0.022\,60 \pm 0.000\,53$) has been deduced from the analysis of the anisotropies in the CMB as observed by the Wilkinson microwave anisotropy probe (WMAP) satellite [1]. Using the best available nuclear reaction rates, this now allows precise predictions to be made for the primordial abundances of these light nuclei. A comparison between calculations and observations reveals good agreement for helium, excellent agreement for deuterium, and a discrepancy (by a factor of $\approx$4) for ^{7}Li [2–4]. Possible reasons for this discrepancy for ^{7}Li have recently been discussed, e.g., by Spite and Spite [5].

In 2006, high-resolution observations of Li absorption lines in some very old halo stars led the authors to claim evidence for large primordial abundances also of the weakly bound isotope ^{6}Li [6]. The ^{6}Li/^{7}Li ratios of $\sim 5 \times 10^{-2}$ were found to be about three orders of magnitude larger than the BBN-calculated value of ^{6}Li/^{7}Li $\sim 10^{-5}$. This observation has triggered many studies to resolve the discrepancy either by considering an early ^{6}Li formation in primitive dwarf galaxies at high redshift in a hierarchical-structure formation context [7] or *in situ* by solarlike flares [8], or in terms of physics beyond the standard model of particle physics (see, e.g., Refs. [9–11]). More recently, however, Cayrel *et al.* [12] and Steffen *et al.* [13] have pointed out that line asymmetries similar to those created by a ^{6}Li blend could also be produced by convective Doppler shifts in stellar atmospheres. Similarly, a recent study of Garcia Perez *et al.* [14] could not claim any significant detection of ^{6}Li in metal-poor stars. So at present the debate is open. More stellar observations are required to solve this question (see Asplund and Lind [15]).

Predictions for the production of ^{6}Li in BBN require precise measurements of the ^{2}H(α,γ)^{6}Li reaction rate, the key production mechanism. In BBN, this reaction occurs at energies in the range $50 \leqslant E_{\mathrm{c.m.}} \leqslant 400$ keV [16]. At higher energies, this reaction has been studied carefully in direct

*Present address: Centro de Física Nuclear, Universidade de Lisboa, P-1649-003 Lisboa, Portugal.

†k.suemmerer@gsi.de

‡Present address: Diakonie-Klinikum Schwäbisch-Hall, D-74523 Schwäbisch-Hall, Germany.

§Present address: GANIL, B.P. 55027, F-14076 Caen Cedex 5, France.

kinematics: at energies above 1 MeV by Robertson *et al.* [17], and by Mohr *et al.* [18] in the energy range around the dominant 3^+ resonance at $E_{\rm c.m.} = 0.711$ MeV. At BBN energies, however, direct measurements are difficult owing to extremely low cross sections (about 29 pb at $E_{\rm c.m.} = 100$ keV). An attempt by Cecil *et al.* [19] at $E_{\rm c.m.} = 0.053$ MeV yielded only an upper limit for the S factor of 2.0×10^{-7} MeV b, which is more than an order of magnitude higher than present estimates. A straightforward solution to overcome this problem is offered by the indirect method of Coulomb dissociation (CD). As will be shown below, the dominant multipolarity involved is $E2$. When a high-Z target like ^{208}Pb is bombarded with a medium-energy ($\approx$150 A MeV)^{6}Li beam, an intense flux of virtual $E2$ photons is created that dissociates ^{6}Li into ^{2}H and α with a greatly enhanced cross section. From the energy-differential CD cross section, the radiative-capture one can be calculated easily [20] provided that the multipolarity of the respective transition is known and that higher-order electromagnetic or nuclear contributions can be either ignored or taken into account quantitatively.

Kiener *et al.* [21] have investigated the ^{2}H$(\alpha,\gamma)^6$Li reaction by means of the CD method employing 26 A MeV ^{6}Li projectiles breaking up into $^2\mathrm{H} + \alpha$ in the Coulomb field of a ^{208}Pb nucleus. Referring to a theoretical paper by Shyam *et al.* [22], Kiener *et al.* claimed that their measurement is largely free from nuclear background (the same assumption was made in a later reevaluation of the same data set [23]). While the astrophysical S factor derived in Ref. [21] seems to agree well with theoretical predictions at and above the resonance, a puzzling result emerged below the resonance: the experimental data suggest a rather constant S factor in the astrophysically interesting region below 400 keV; most theoretical curves, however, drop with decreasing energy [24]. As we will show in the present paper, it is likely that this constant S factor is due to nuclear processes that cannot be ignored.

We report in this article on a new breakup measurement performed at the SIS-18 heavy-ion synchrotron at GSI (Helmholtzzentrum für Schwerionenforschung in Darmstadt, Germany) using a higher-energy (150 A MeV)^{6}Li beam. This higher beam energy should have several advantages compared to the one used by Kiener *et al.*: (i) the stronger forward focusing allows for a more complete angular coverage; (ii) CD should be enhanced relative to the nuclear contribution. In addition, we have developed a comprehensive theoretical model of electromagnetic and nuclear breakup processes that allows us to interpret the measured data in detail. We will show below, however, that it is unfortunately not possible to separate experimentally the electromagnetic and nuclear contributions. Nevertheless, most of the features of the measured data can be well explained by our model, thus giving our calculated ^{2}H$(\alpha,\gamma)^6$Li cross sections a firm experimental basis.

II. THEORETICAL PREDICTIONS

A. Radiative-capture reaction

The cross section of the ^{2}H$(\alpha,\gamma)^6$Li reaction at energies $E_{\rm c.m.} < 1$ MeV is dominated by radiative $E2$ capture from d waves in the $\alpha + {}^2$H channel into the $J^\pi = 1^+$ ground state of ^{6}Li via a prominent 3^+ resonance at $E_{\rm c.m.} = 0.711$ MeV. In comparison, $E1$ transitions from p waves to the ^{6}Li ground state are strongly suppressed by the isospin selection rule for $N = Z$ nuclei because of the almost equal charge-to-mass ratio of the deuteron and the α particle. Only at very low energies ($E_{\rm c.m.} \leqslant 150$ keV) is the $E1$ contribution expected to become larger than the $E2$ capture since the penetrabilities in p and d waves exhibit a different energy dependence [17].

In the past, a number of different theoretical approaches were considered for the calculation of the low-energy ^{2}H$(\alpha,\gamma)^6$Li capture cross section; see [24] and references therein. They comprise, e.g., simple potential models and microscopic cluster models using the resonating group method or the generator coordinate method. Provided that the parameters of these models are well fitted to observable quantities like the binding and resonance energies in the ^{6}Li system and that the asymptotic form of the bound state wave function is correctly taken into account, good agreement between the predictions for the low-energy cross section is found. This shows that the radiative capture at energies below the 3^+ resonance is essentially an extranuclear process and that details of the interior wave function are less important.

In the present work we employ a potential model for the ^{6}Li system that provides the S factor for the ^{2}H$(\alpha,\gamma)^6$Li reaction and, at the same time, can be used in modeling the breakup reaction when ^{6}Li is scattered on a Pb nucleus at 150 A MeV. This model assumes that ^{6}Li is described by two interacting clusters, α and ^{2}H, without internal structure. Bound and scattering wave functions in the relevant partial waves, characterized by orbital angular momentum l and total angular momentum J, are obtained by solving the appropriate radial Schrödinger equation with α-^{2}H potentials that contain a central part of Woods-Saxon form,

$$V_c^{l,J}(r) = -\mathcal{V}_c^{l,J}\left[1 + \exp\left(\frac{r-R}{a}\right)\right]^{-1}, \qquad (1)$$

and a spin-orbit part of derivative Woods-Saxon form,

$$V_{\rm so}^{l,J}(r) = \mathcal{V}_{\rm so}^{l,J}\lambda^2 \frac{\vec{L}\cdot\vec{S}}{\hbar^2 r}\frac{d}{dr}\left[1 + \exp\left(\frac{r-R}{a}\right)\right]^{-1}, \qquad (2)$$

with $\lambda = 2$ fm. The radius R is given by $R = 1.25\,A^{1/3}$ fm with $A = 6$; $a = 0.65$ fm denotes the diffuseness parameter. The depths $\mathcal{V}_c^{l,J}$ were set to 60.712 MeV for the ground state ($l = 0$) and 56.7 MeV for all other partial waves ($l = 1,2$). For the spin-orbit part $\mathcal{V}_{\rm so}^{l,J}$ a depth of 2.4 MeV was used for the relevant partial waves $l = 1,2$. These values were obtained by adjusting the parameters so as to reproduce the experimental values for the binding energy $E_B = 1.474$ MeV of ^{6}Li and the 3^+ resonance energy with respect to the $\alpha + {}^2$H threshold. This choice of parameters also describes the low-energy α-^{2}H experimental scattering phase shifts very well; see Fig. 1.

The cross section of the radiative-capture reaction is calculated in the present model with the usual long-wavelength approximation of the $E1$ and $E2$ multipole operators $\mathcal{M}(E\lambda\mu) = Z_{\rm eff}^{(\lambda)} e r_{\alpha D}^{\lambda} Y_{\lambda\mu}(\hat{r}_{\alpha d})$ where e denotes the electron charge and $\vec{r}_{\alpha d}$ is the radius vector between α and the deuteron.

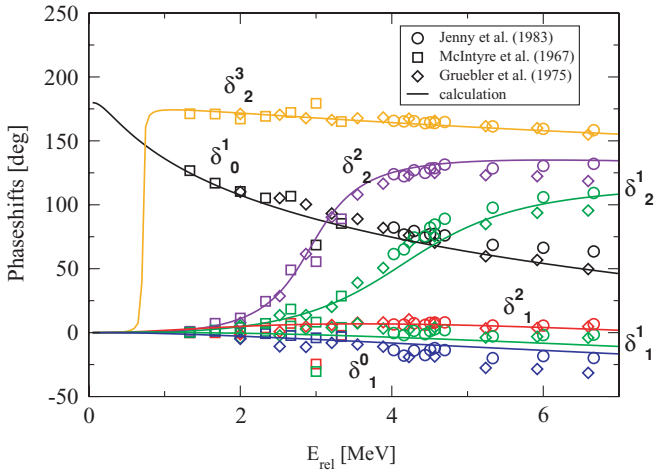

FIG. 1. (Color online) Phase-shift data measured for low-energy α-^{2}H scattering as a function of the relative α-^{2}H energy in the c.m. system, $E_{\rm rel}$. Data points are from Jenny *et al.* (circles, [25]), McIntyre and Haeberli (squares, [26]), and Grüebler *et al.* (diamonds, [27]). The results of the model calculations (full lines) were obtained with the potential parameters described in the text.

The effective charge numbers

$$Z_{\rm eff}^{(\lambda)} = Z_d \left(\frac{m_\alpha}{m_d + m_\alpha}\right)^\lambda + Z_\alpha \left(-\frac{m_d}{m_d + m_\alpha}\right)^\lambda \qquad (3)$$

depend on the charge numbers Z_i and masses m_i of the two clusters. The $E1$ effective charge number does not vanish since experimental values for the masses are used. However, the $E2$ contribution dominates over most of the range of energies with a pronounced peak at the position of the 3^+ resonance. Only at energies below 110 keV does the $E1$ contribution exceed the $E2$ contribution. We display the energy dependences of the two relevant multipole contributions to the S factor below in Fig. 9 of Sec. IV.

B. Breakup reaction

The theoretical description of the breakup reaction ^{208}Pb(^{6}Li,α^2H)^{208}Pb is considerably more involved than that of the radiative-capture reaction, in particular if both electromagnetic and nuclear breakup have to be included. The differential breakup cross section in the ^{6}Li-^{208}Pb c.m. system can be written in the general form

$$\frac{d^3\sigma}{d\Omega_{\rm LiPb} dE_{\alpha d} d\Omega_{\alpha d}} = \frac{\mu_{\rm LiPb}^2}{(2\pi)^2\hbar^4}\frac{p_{\rm LiPb}^f}{p_{\rm LiPb}^i}\frac{1}{2J_{\rm Li}+1}\sum_{M_{\rm Li}}\sum_{M_d}|T_{fi}|^2\frac{\mu_{\alpha d}\, p_{\alpha d}}{(2\pi\hbar)^3} \qquad (4)$$

with reduced masses $\mu_{ij} = m_i m_j/(m_i + m_j)$ and relative momenta $\vec{p}_{ij} = \mu_{ij}(\vec{p}_i/m_i - \vec{p}_j/m_j)$. Ω_{ij} denotes the solid angle for the scattering of particles i and j in their c.m. system and $E_{\alpha d} = p_{\alpha d}^2/(2\mu_{\alpha d})$ is the c.m. energy in the fragment system after the breakup. In the initial state, ^{6}Li is in the ground state with total angular momentum $J_{\rm Li} = 1$ and $M_{\rm Li} = \pm 1,0$. In the final state, the deuteron carries spin 1 with projections $M_d = \pm 1,0$. The cross section (4) determines the relative probability to find the two fragments with given momenta in the final state and thus can be used directly in a Monte Carlo simulation of the breakup reaction.

The main task is to calculate the T matrix element that contains all the relevant information on the breakup process. In the distorted wave Born approximation it is given by

$$T_{fi} = \left\langle \chi^{(-)}(\vec{p}_{\rm LiPb}^{\,f})\Psi_{\alpha d}^{(-)}(\vec{p}_{\alpha d} M_d)\right| \times (V_{\rm LiPb} - U_{\rm LiPb})\left|\Phi_{\rm Li}(J_{\rm Li} M_{\rm Li})\chi^{(+)}(\vec{p}_{\rm LiPb}^{\,i})\right\rangle \qquad (5)$$

with the ^{6}Li ground state wave function $\Phi_{\rm Li}$ and the wave function $\Psi_{\alpha d}^{(-)}$ for the relative motion of the fragments in the continuum. These two functions are given by the solutions of the Schrödinger equation as in the calculation of the radiative-capture cross section. The distorted waves $\chi^{(\pm)}$ describe the scattering of the projectile on the target. They can be found by solving the Schrödinger equation for the Li-Pb scattering with the optical potential $U_{\rm LiPb}$ which depends only on the distance between Li and Pb. In contrast, $V_{\rm LiPb}$ is the full many-body interaction potential. It is approximated by

$$V_{\rm LiPb} \approx \frac{Z_\alpha Z_{\rm Pb} e^2}{|\vec{r}_\alpha - \vec{r}_{\rm Pb}|} + \frac{Z_d Z_{\rm Pb} e^2}{|\vec{r}_d - \vec{r}_{\rm Pb}|} + U_{\alpha{\rm Pb}}^N(|\vec{r}_\alpha - \vec{r}_{\rm Pb}|) + U_{d{\rm Pb}}^N(|\vec{r}_d - \vec{r}_{\rm Pb}|), \qquad (6)$$

separating Coulomb and nuclear contributions and introducing nuclear optical potentials $U_{\alpha{\rm Pb}}^N$ and $U_{d{\rm Pb}}^N$ for the α-Pb and ^{2}H-Pb interactions, respectively. Similarly, we have

$$U_{\rm LiPb}(\vec{r}_{\rm LiPb}) \approx \frac{Z_{\rm Li} Z_{\rm Pb} e^2}{|\vec{r}_{\rm LiPb}|} + U_{\rm LiPb}^N(|\vec{r}_{\rm LiPb}|) \qquad (7)$$

with $\vec{r}_{\rm LiPb} = \vec{r}_{\rm Li} - \vec{r}_{\rm Pb}$. Since both potentials contain Coulomb and nuclear contributions additively, it is possible to separate the T matrix element into a Coulomb and a nuclear part as

$$T_{fi} = T_{fi}^C + T_{fi}^N. \qquad (8)$$

In general, Coulomb and nuclear contributions to the breakup amplitude can interfere.

In the breakup experiment, the projectile velocity $v_{\rm LiPb}$ relative to the target is large and the fragments are observed at small forward scattering angles with respect to the beam axis. Thus it is sufficient to replace the distorted waves appearing in Eq. (5) by their eikonal approximation, i.e.,

$$\chi^{(-)*}(\vec{p}_{\rm LiPb}^{\,f})\chi^{(+)}(\vec{p}_{\rm LiPb}^{\,i}) = \exp[i\vec{q}\cdot\vec{b}]\exp[i\,S_{\rm LiPb}(\vec{b})] \qquad (9)$$

with the momentum transfer

$$\vec{q} = \frac{1}{\hbar}(\vec{p}_{\rm LiPb}^{\,i} - \vec{p}_{\rm LiPb}^{\,f}) \qquad (10)$$

and the phase function

$$S_{\rm LiPb}(\vec{b}) = -\frac{1}{\hbar v_{\rm LiPb}}\int_{-\infty}^{\infty} dz\, U_{\rm LiPb}(\vec{r}_{\rm LiPb}), \qquad (11)$$

where the coordinate vector has been decomposed as

$$\vec{r}_{\rm LiPb} = \vec{b} + z\hat{e}_{\rm beam}, \qquad \vec{b} \perp \hat{e}_{\rm beam}, \qquad (12)$$

and $\hat{e}_{\rm beam}$ denotes the beam direction. The Coulomb part of the phase function can be calculated analytically. In order to avoid a divergent result at small impact parameters b, the Coulomb

potential of a pointlike target charge in Eq. (7) is replaced by that of a homogeneous sphere. In the eikonal approximation, the Coulomb and nuclear T matrix elements can be written as

$$T_{fi}^{C/N} = \langle \Psi_{\alpha d}^{(-)}(\vec{p}_{\alpha d} M_d) | F_{C/N}(\vec{r}_{\alpha d}) | \Phi_{\rm Li}(J_{\rm Li} M_{\rm Li}) \rangle \quad (13)$$

with the Coulomb form factor

$$F_C(\vec{r}_{\alpha d}) = Z_{\rm Pb} e \int d^3 r_{\rm LiPb} \exp[i\vec{q}\cdot\vec{b}] \exp[i S_{\rm LiPb}(\vec{b})] \times \left(\frac{Z_\alpha e}{|\vec{r}_{\alpha \rm Pb}|} + \frac{Z_d e}{|\vec{r}_{d\rm Pb}|} - \frac{Z_{\rm Li} e}{|\vec{r}_{\rm LiPb}|} \right) \quad (14)$$

and the nuclear form factor

$$F_N(\vec{r}_{\alpha d}) = \int d^3 r_{\rm LiPb} \exp[i\vec{q}\cdot\vec{b}] \exp[i S_{\rm LiPb}(\vec{b})] \times \left(U_{\alpha \rm Pb}^N + U_{d\rm Pb}^N - U_{\rm LiPb}^N \right) \quad (15)$$

which can both be decomposed into multipoles $L = 0,1,2,\ldots$. Using the method of steepest descent, the multipole components of the Coulomb form factor (14) are easily calculated. Neglecting the nuclear contribution in the phase function $S_{\rm LiPb}$, one obtains in lowest order the well-known Coulomb excitation functions in the semiclassical approximation. The nuclear optical potential $U_{\rm LiPb}^N$ in (11) leads to corrections that take, e.g., the absorption by the target nucleus into account; also, relativistic corrections are easily included (see Ref. [28] for details).

Since the $E2$ virtual photons are orders of magnitude more abundant than the $E1$ ones, the Coulomb contribution to the breakup is essentially sensitive only to the quadrupole contribution. (There is no monopole contribution in this case.) In contrast to electromagnetic $E1$ excitations, nuclear $L = 1$ excitations are not suppressed by isospin selection rules. Nuclear processes for all multipolarities have, therefore, to be taken into account when modeling the breakup of ^{6}Li into $\alpha + {}^2$H at about 150 A MeV. In the present work, we included nuclear $L = 0, 1, 2$ excitations because higher multipoles are expected to give only small contributions to the total breakup amplitude.

In order to obtain numerical results for the T matrix elements, one has to specify the nuclear optical potentials that enter into the calculation. Unfortunately, there are no systematic optical-model potentials available describing the elastic scattering of α, ^{2}H, and ^{6}Li on a Pb target at 150 A MeV. Therefore, we generated the optical potentials from systematic optical-model potentials for nucleon-Pb elastic scattering and folded them with the matter distribution of the projectile and the fragments, respectively. These potentials were tuned to reproduce published elastic-scattering data at incident energies as close to 150 A MeV as possible by multiplying the real and imaginary parts by scaling factors not too far from unity. Literature data have been used for the elastic scattering of ^{2}H + ^{208}Pb at 55 and 70 A MeV [29,30], of α + ^{208}Pb at 120 A MeV and 175 A MeV [31], and of ^{6}Li + ^{208}Pb at 100 A MeV [32].

We found that deuteron and α scattering on Pb were best described starting with the relativistic nucleon-nucleus potentials of Ref. [33]. In the case of ^{6}Li-Pb scattering the non-relativistic optical-model potential from Ref. [34] for nucleon-nucleus scattering worked best. Figure 2 shows measured and fitted elastic-scattering data for the three cases. The optical-model potentials, obtained by the procedure described above for the actual energy of the breakup experiment, are well fitted by a Woods-Saxon shape. Since mostly the outer region of the potential is important the fits were started at a radius of 7 fm. In Table I we give the numerical values of the depth, radius, and diffuseness parameters for the real and imaginary parts.

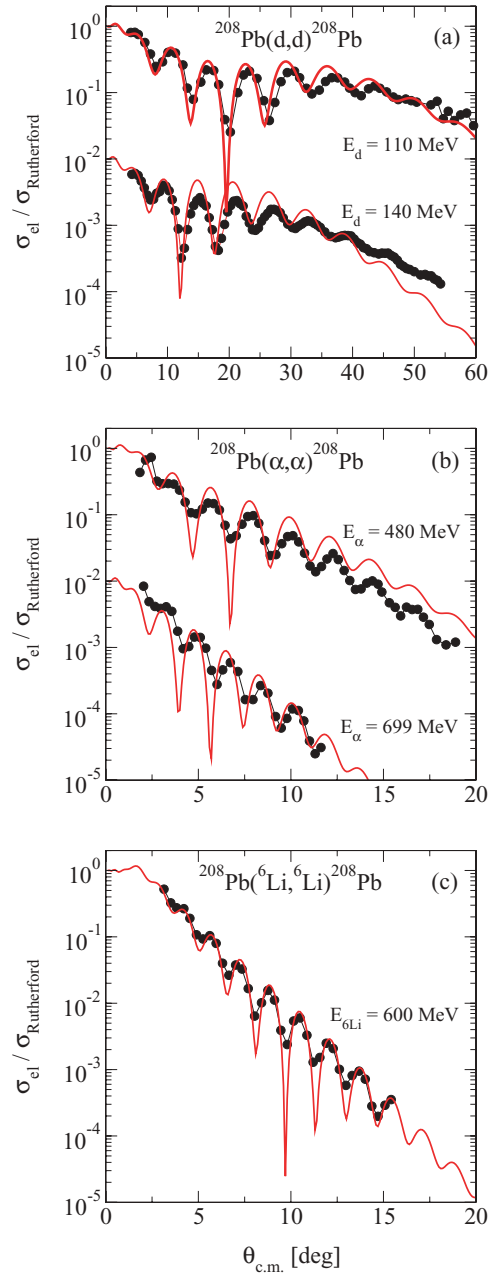

FIG. 2. (Color online) Center-of-mass angular distributions for (a) 55 and 70 A MeV ^{2}H, (b) 120 and 175 A MeV α, and (c) 100 A MeV ^{6}Li on ^{208}Pb. The full lines represent fits to the measured data using the optical-model potentials as described in the text. Note that the angular distributions for $E_d = 140$ MeV in (a) and for $E_\alpha = 699$ MeV in (b) have been scaled by a factor of 10^{-2}.

TABLE I. Woods-Saxon potential parameters used to describe the scattering of ^{6}Li, α, and ^{2}H on a Pb target.

System	^{6}Li + ^{208}Pb	α + ^{208}Pb	^{2}H + ^{208}Pb
V_{real} (MeV)	55.0407	48.0315	23.6250
R_{real} (fm)	7.4979	7.9014	7.9057
a_{real} (fm)	0.8665	0.8542	0.8984
V_{imag} (MeV)	84.1720	45.4504	28.3867
R_{imag} (fm)	7.3633	7.3763	7.3712
a_{imag} (fm)	0.8693	0.9020	0.9391

C. Predicted observables

The most meaningful observable that can illustrate the predictions from the above-sketched model of ^{6}Li breakup is the scattering angle θ_6 of the excited ^{6}Li* before breakup, relative to the incoming ^{6}Li beam. Figure 3 depicts the expected θ_6 distribution.

The figure clearly shows that pure nuclear, pure Coulomb, and total (CD + nuclear) distributions exhibit distinctly different peak structures. Pure Coulomb interaction has its most prominent peak where the other contributions show a minimum. Likewise, the total (CD + nuclear) distribution can be distinguished from a nuclear-only theory by the large amplitude of the most prominent peak (because of constructive CD-nuclear interference), and by the disappearance of the third maximum (because of destructive interference). In principle, these features should allow separation of the contributions from the individual interactions. However, the theoretical predictions have to be folded with the resolution and the acceptance of the experimental apparatus using the Monte Carlo simulations described below in Sec. III B.

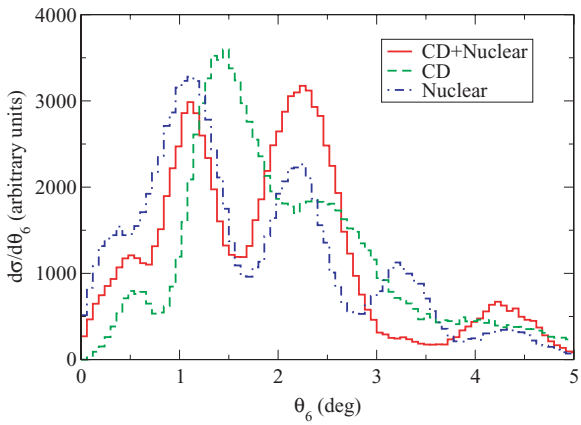

FIG. 3. (Color online) Expected distribution of the differential cross section $d\sigma/d\theta_6$ as a function of the scattering angle θ_6 of the excited ^{6}Li* before breakup, in arbitrary units. The full (red) curve represents the total distribution, whereas the nuclear and Coulomb contributions are depicted by the dot-dashed (blue) and dashed (green) histograms, respectively. Note that the different curves have been normalized to the same total cross section. All distributions were summed over ^{2}H-α c.m. energies E_{rel} up to 1.5 MeV.

III. EXPERIMENTAL PROCEDURE

A. Apparatus

A schematic view of the setup used is given in Fig. 4. A ^{208}Pb target with 200 mg/cm^2 thickness was bombarded by a primary ^{6}Li beam of 150 A MeV energy. The ^{6}Li beam was produced by the SIS-18 synchrotron at GSI, separated from possible contaminant ions by using the FRS fragment separator [35] and transported to the standard target position of the kaon spectrometer KaoS [36]. The average ^{6}Li beam intensity at the breakup target was of the order of 5×10^4 per 4 sec spill. The beam had a width of 0.17 (0.12) cm and an angular divergence of 4.4 (4.4) mrad in the x (y) direction at the target (1σ widths).

The angles and positions as well as the energy losses of the outgoing particles, ^{2}H and α, were measured by two pairs of single-sided silicon strip detectors (SSDs, 300 μm thick, 100 μm pitch) [37] placed at distances of 15 and 30 cm, respectively, downstream from the target. From the detector pitch one can calculate a resolution of the ^{2}H-α opening angle in the laboratory, θ_{24}, of about 1%. Noninteracting ^{6}Li beam particles were identified event by event with a 16-strip ΔE detector located directly behind the SSDs and stopped in a cylindrical Ta absorber (12 mm diameter, 20 mm length) placed behind the detector. Breakup events were discriminated from noninteracting ^{6}Li-beam events by their energy-loss signals in the 16-strip ΔE detector; an energy loss corresponding to ^{6}Li was used as a trigger veto signal. Deuteron and α momenta were analyzed with the large-acceptance KaoS spectrometer and were detected in two consecutive multiwire proportional chambers (MWPCs) [37] followed by a plastic-scintillator time-of-flight (TOF) wall consisting of 30 elements (each 7 cm wide and 2 cm thick). This plastic wall was used as a trigger detector for the data acquisition system. The KaoS magnets' volume was filled with He gas at atmospheric pressure to reduce multiple scattering.

The coincident ^{2}H and α fragments resulting from breakup in the ^{208}Pb target were identified by reconstructing their vertex at the target. This removed all breakup events in layers of matter other than the target. The ^{2}H and α momenta were determined from tracking them with GEANT through the MWPCs and TOF wall behind KaoS. The incident angles in front of the magnets were known unambiguously from the SSD hits. While in the SSDs each hit could be attributed to either ^{2}H or α by its energy deposition, the corresponding hits in the MWPCs were attributed to the respective particle type by finding the optimum trajectory through the MWPCs and the TOF wall. This was done in an iterative procedure that started with a test assignment of each hit to either α or ^{2}H and a test momentum for each of them. Both the momentum values and the assignments were then iteratively changed until the minimum squared deviation from the observed hits in all detectors downstream from the KaoS magnet was reached. This momentum reconstruction could be shown to be accurate within about 10^{-3}. From the opening angles between the fragments and from their momenta, the relative energies E_{rel} between the ^{2}H and α particles in the c.m. system could be reconstructed.

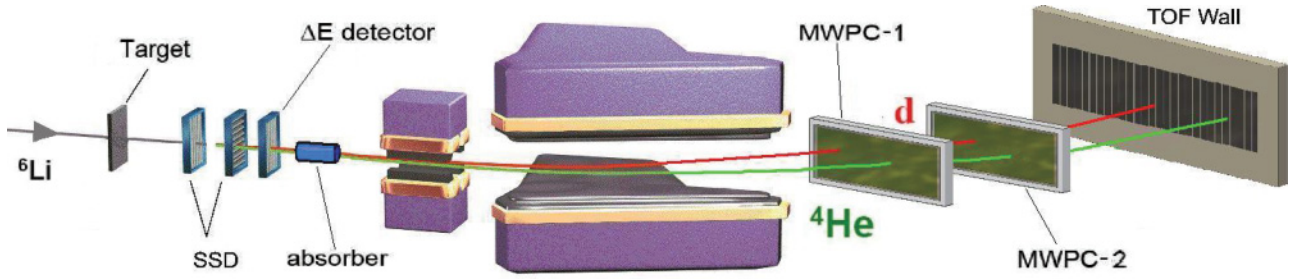

FIG. 4. (Color online) The experimental setup shows the fragment-tracking SSD behind the Coulomb-breakup target followed by a 16-strip ΔE detector and a beam stopper. Deuteron and α positions were measured near the focal plane of the KaoS QD spectrometer by two successive large-area multiwire proportional chambers (MWPCs) followed by a scintillator-paddle TOF wall used for trigger purposes.

B. Monte Carlo simulations

It is obvious that the experimental apparatus imposes strong restrictions on the detection of the breakup particles, α and ^{2}H. This applies in particular to the angular acceptance, the energy and position resolution, and the detection efficiency. As a consequence, a meaningful comparison between theoretical predictions and experimental data can only be made using theoretical data filtered by the experimental setup. To this end, we have modeled the entire setup, starting in front of the ^{208}Pb breakup target, in GEANT3 [38]. As an event generator, the theoretical model described in the previous section was used. Input data were generated as statistically distributed ensembles of 100 000 breakup "events" each that were distributed according to the calculated differential cross sections. The emittance of the ^{6}Li beam (as measured without breakup target and without absorber) was imposed. Each breakup particle, α and ^{2}H, was followed through the remainder of the Pb target after the reaction vertex, the SSD detectors, the beamline exit window, the He-filled interior of the magnets with the magnetic field, and the air behind KaoS before hitting the MWPC volumes and the TOF wall.

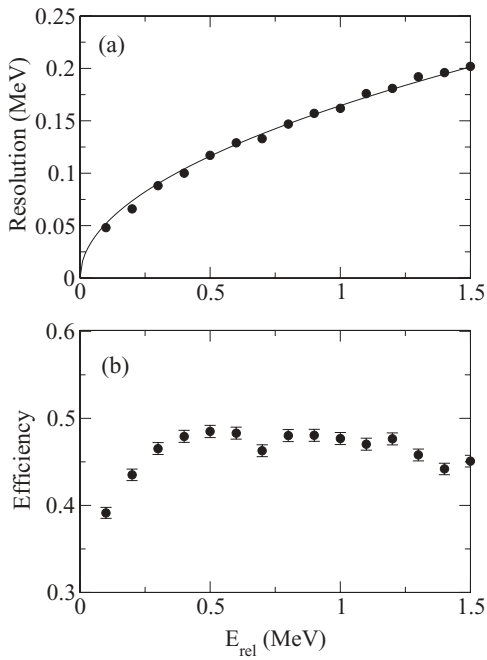

FIG. 5. (a) Relative-energy resolution (1σ widths) as determined by simulating ^{6}Li breakup with GEANT. The data points can be approximated by the fitted function $\sigma_E = 0.1645 \times \sqrt{E_{\rm rel}}$. (b) Combined geometrical and analysis efficiency of determining $E_{\rm rel}$ from the ^{2}H and α momentum vectors. The intrinsic efficiency of the MWPC detectors has been assumed to be unity in this graph.

The Monte Carlo simulations were used to obtain estimates of the resolution and the efficiency of our setup. As an example, we plot in Fig. 5(a) the 1σ resolution of $E_{\rm rel}$. The data points were obtained by sending 10 000 events each with different values of $E_{\rm rel}$ (within a narrow bin of 0.1 MeV width for each case) into our setup and analyzing the outgoing particles with the same routines as in the experiment. From the same data sets, the number of counts gave an approximate estimate of the detection efficiency, shown in Fig. 5(b). In the experiment, however, the detection efficiency is additionally limited by the small and strongly fluctuating energy deposition of deuterons in the MWPCs. This latter quantity cannot be simulated easily, such that we had to normalize the number of observed and simulated counts. Therefore, our experiment does not allow us to determine absolute cross sections, despite the fact that all incident ^{6}Li ions were counted.

IV. EXPERIMENTAL RESULTS

A relatively unbiased observable, based only on high-resolution SSD measurements, is the opening angle θ_{24} between the outgoing fragments ^{2}H and α. Figure 6 shows this distribution, summed over $E_{\rm rel}$ values up to 1.5 MeV; this condition was also set for all other spectra shown below. The experimental data points are compared with the corresponding Monte Carlo simulations for pure Coulomb (CD) and pure nuclear interactions as well as combined (CD + nuclear) interactions. Each simulated histogram was normalized to contain the same number of counts as the experimental spectrum, thus providing the single scaling factor used to normalize all simulated distributions.

As seen in Fig. 6, the data are reasonably well reproduced by the simulations over their entire range. The 3^+ resonance peak is clearly visible around 3°; its angular width is well reproduced indicating that the simulation takes both the scattering and the finite angular resolution well into account.

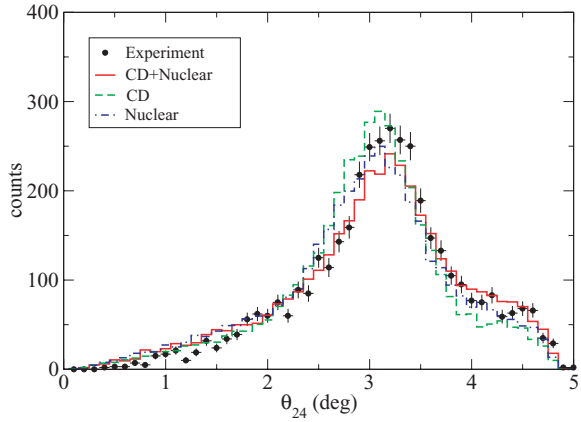

FIG. 6. (Color online) Opening angles θ_{24} between the outgoing fragments ^{2}H and α. Full circles correspond to measured data. The dash-dotted histogram (blue) denotes simulations with pure nuclear interaction, whereas the pure CD contribution is shown by the dashed histogram (green). Combined (CD + nuclear) contributions are shown by the full red line. Note that the numbers of simulated counts in each spectrum were normalized to the experimental ones.

It is obvious, however, that one cannot distinguish between the different interactions on the basis of this angular distribution. We have therefore to search for an observable that is more sensitive to the type of interaction. In Fig. 3 above, we have shown that the observable θ_6 should be very sensitive to the type of interaction.

The experimental data for this observable are presented in Fig. 7. Figure 7(a) shows data for $E_{\rm rel}$ values below the resonance; Fig. 7(b) covers the resonance region, whereas Fig. 7(c) has been plotted for $0.9 \leqslant E_{\rm rel} < 1.5$ MeV. The finite KaoS acceptance cuts the distributions at about 4°. The figure shows clearly that the observable θ_6 is sensitive to the type of interaction. In all panels, the combined (CD + nuclear) interaction, including interference, reproduces most of the structures observed in the data points (red histograms). This is particularly true for the subresonance region, Fig. 7(a). The green histograms (CD-only) show single peaks at larger angles. The pure nuclear interaction (blue histograms) rises rapidly at small values of θ_6, in agreement with the measured data, but lacks the structures visible in the data points. The narrow peaks visible in the on-resonance data, Fig. 7(b), at values of θ_6 of ≈1.5°, 2.6°, and 3.3°, are not perfectly reproduced by the (CD + nuclear) model and point to small deficiencies of the theoretical model. Nevertheless, Fig. 7 demonstrates that Coulomb-nuclear interference is at work and that the signs of the interference terms are correct. We also conclude that even at our incident energy of 150 A MeV the nuclear breakup is dominant.

The angle-integrated energy-differential cross sections as a function of $E_{\rm rel}$ are shown in Fig. 8. The full histogram was obtained from the (CD + nuclear) calculation convoluted by our GEANT simulation and normalized to the experimental yield. The points and the histogram represent the measured and predicted differential cross sections, respectively, as a function of $E_{\rm rel}$. Our $E_{\rm rel}$ distribution is in very good agreement with

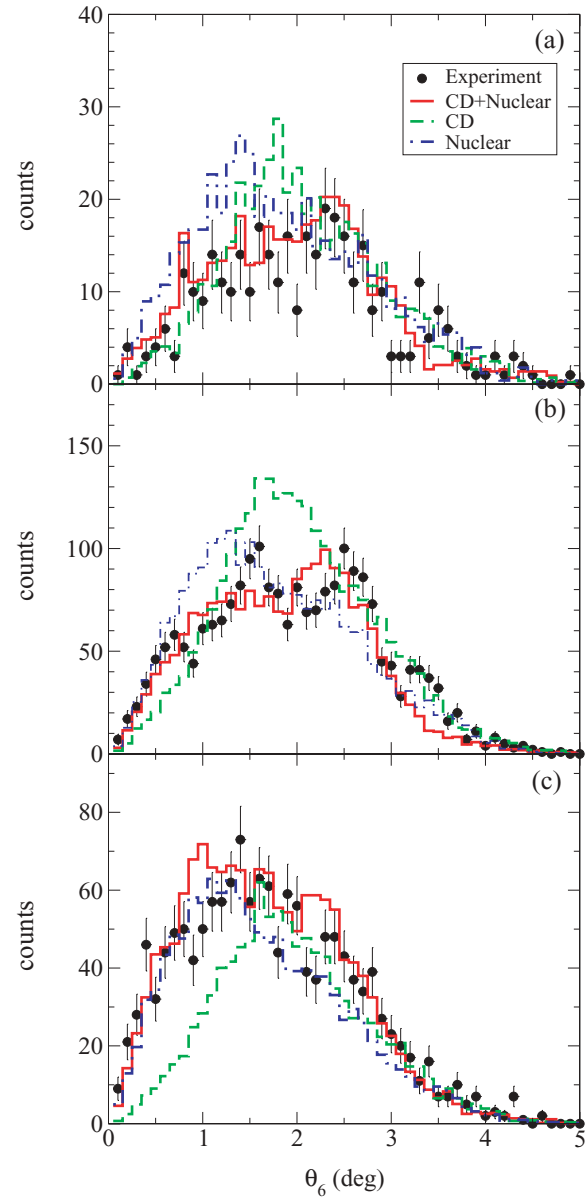

FIG. 7. (Color online) Angular distribution of the excited ^{6}Li* nuclei after the reaction (θ_6). The panels represent three different bins of $E_{\rm rel}$: (a) $0.0 \leqslant E_{\rm rel} < 0.5$ MeV; (b) $0.5 \leqslant E_{\rm rel} < 0.9$ MeV; (c) $0.9 \leqslant E_{\rm rel} < 1.5$ MeV. The measured data points are shown in comparison with simulations with pure nuclear and pure CD as well as with (CD + nuclear) interactions. Line types and color codes are identical to the ones in Fig. 6.

the simulation in particular in the energy region below 400 keV. As we will show below (see Fig. 10), the differential cross sections in this energy regime result mostly from nuclear interactions.

The astrophysically important quantity is the astrophysical S factor S_{24} for the ^{2}H$(\alpha,\gamma)^6$Li reaction. Since nuclear processes dominate, in particular for low $E_{\rm rel}$, the determination of this quantity via an evaluation of the CD component in our breakup data is not feasible. However, we have demonstrated above that our theoretical model describes well the measured cross sections; hence the astrophysical S

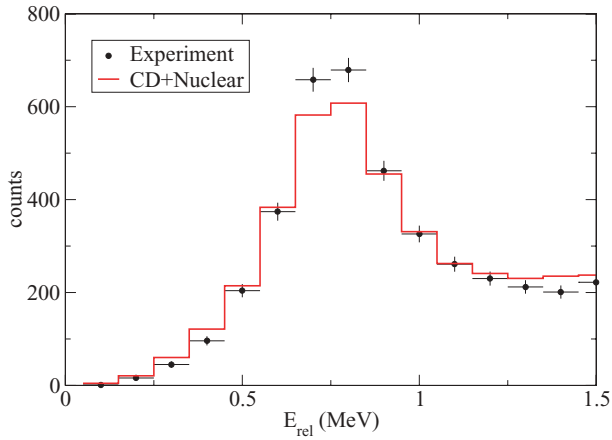

FIG. 8. (Color online) Differential cross sections as a function of the energy E_{rel} in the α-^{2}H c.m. system. Black points indicate the experimental data; the histogram corresponds to the GEANT simulation using the (CD + nuclear) interaction as described in the text and a binning of 100 keV (note that the vertical error bars result from a quadratic sum of statistical and systematical uncertainties).

factors from the present work are those from our theoretical model.

The resulting $E1$, $E2$, and total S_{24} factors are visualized in the upper part of Fig. 9 together with the previous CD data of Kiener *et al.* [21] and the direct data of Mohr *et al.* [18] and Robertson *et al.* [17]. The present results for the $E2$ component are in good agreement with the direct measurements of Refs. [17,18] in the resonance region and above, which gives confidence in our model.

Another check of the validity of our treatment of the Coulomb part of the breakup reaction, described in Sec. II A, can be done by comparing our calculated resonance parameters for the 3^+ resonance with the experimental ones. In order to determine those parameters, we have calculated the theoretical capture cross section around the resonance in 1 keV steps and fitted a Breit-Wigner parametrization to the resonance. We obtain Γ widths of $\Gamma_\alpha = 22.1$ keV and $\Gamma_\gamma = 0.437$ meV, in good agreement with the literature values of $\Gamma_\alpha = 24 \pm 2$ keV and $\Gamma_\gamma = 0.440 \pm 0.030$ meV as cited by Mohr *et al.* [18]. Note that we have used a spectroscopic factor of unity. We will comment on the data points from the previous CD experiment [21] in the following section.

The direct ^{2}H$(\alpha,\gamma)^6$Li reaction at very low energies is sensitive also to the $E1$ amplitude. In our experiment, this component cannot be constrained experimentally due to the weak flux of virtual $E1$ photons. We have therefore to rely exclusively on the theoretical model. At higher energies, however, Robertson *et al.* [17] could separate $E1$ and $E2$ components on the basis of measured angular distributions. Figure 1 in [17] shows that their theory seems to overestimate the $E1$ component. Our $E1$ curve is very close to Robertson *et al.*'s so that we also seem to overestimate this component.

Several theoretical models for ^{6}Li have been proposed to determine the shape and the magnitude of the S_{24} energy dependence, such as potential models [18,28,39], cluster-model calculations [24], or *ab initio* calculations [40]. Those

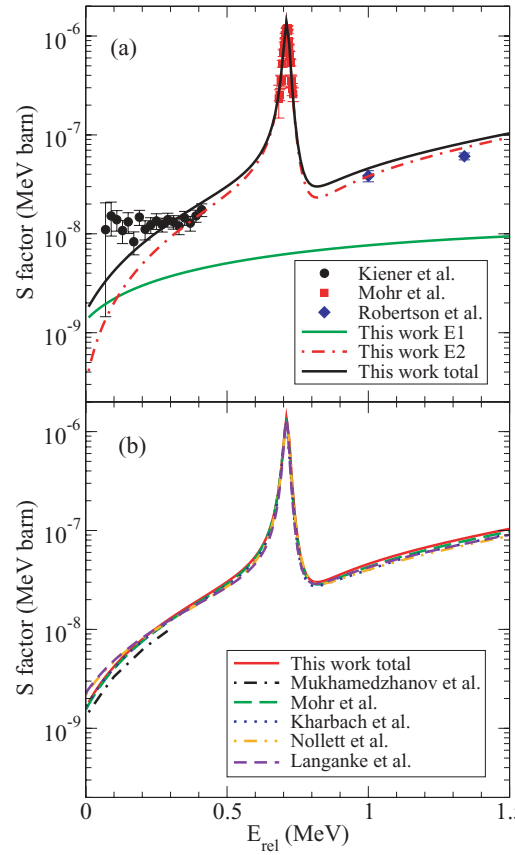

FIG. 9. (Color online) (a) Theoretical $E1$, $E2$, and total S_{24} factors that describe well the present experimental data, together with data points from the previous CD experiment by Kiener *et al.* [21] and from direct measurements (Robertson *et al.* [17] and Mohr *et al.* [18]). See Sec. V for an interpretation of the data of Ref. [21]. (b) Comparison of various theoretical predictions for the summed $E1$ and $E2$ contributions to $S_{24}(E)$ [18,24,39–41].

predicted curves for S_{24} which include both $E1$ and $E2$ contributions are displayed together with the theoretical curve from this work in the lower panel of Fig. 9. As one can see in this figure, all the calculations shown—independent of their very different model assumptions—yield very similar curves. We have not included the theory of Blokhintsev *et al.* [42] because it was specifically tuned to approach the experimental data of Ref. [21].

V. COMPARISON WITH OTHER CD EXPERIMENTS

As visible in the upper panel of Fig. 9, the low-energy data points derived for the S_{24} factor from the work of Kiener *et al.* [21] disagree with the theoretical curve that we have deduced from the present work. We believe that this is most likely due to a strong nuclear contribution at the lower incident energy of 26 A MeV, which was not considered in their analysis in view of the theoretical prediction [22]. We have performed a calculation with the theoretical model of this work at an incident energy of 26 A MeV and have calculated CD and nuclear cross sections for the laboratory angular range between

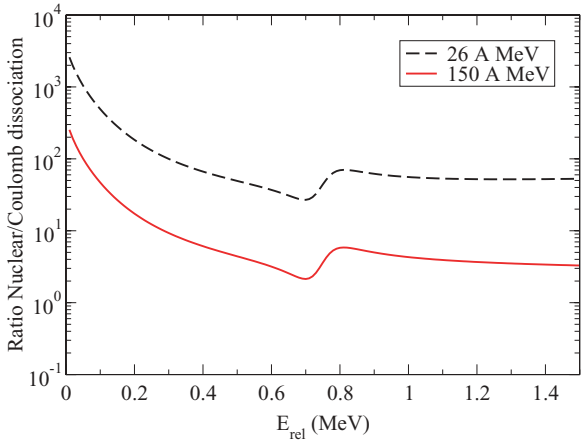

FIG. 10. (Color online) Ratio of nuclear and Coulomb differential dissociation cross sections for ^{6}Li at 150 A MeV (full line) and at 26 A MeV (dashed line). Both curves were calculated with the same model described in detail above in Sec. II B.

1.5° and 6°, which should correspond approximately to the acceptance of the setup of Ref. [21]. Figure 10 displays the ratio of nuclear to Coulomb breakup cross sections as a function of $E_{\rm rel}$ for the two bombarding energies. Our theory predicts that at 150 A MeV the nuclear cross sections are about a factor of 3 larger than the CD ones at and above the resonance, whereas the nuclear component dominates strongly at the lowest energies. At 26 A MeV, the ratio of nuclear to CD cross sections is predicted to be about a factor of 10 larger than at 150 A MeV over the entire range of $E_{\rm rel}$. This suggests that the data points shown in Ref. [21] result almost exclusively from nuclear interactions, contrary to the assumptions underlying the analysis of the authors of [21]. It is therefore not very meaningful to tune theoretical models in order to improve their agreement with the 26 A MeV data as was done in Ref. [42].

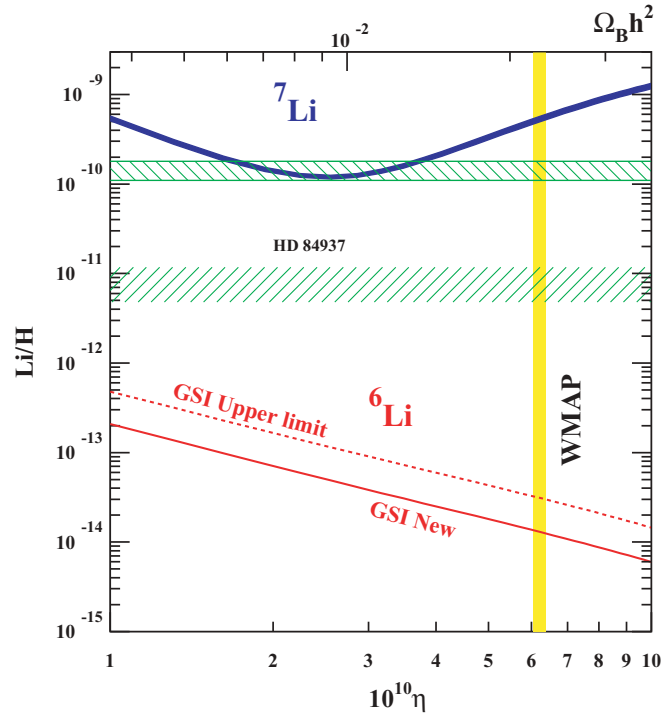

FIG. 11. (Color online) Predicted BBN production ratios for ^{6,7}Li over hydrogen as a function of η, the baryon-to-photon ratio in the early Universe. The solid red line represents the result for ^{6}Li from the S_{24} values obtained in the present work, based on theoretical values for the $E1$ and $E2$ components. The dashed red line represents a very conservative but safe upper limit where all observed events are assumed to result from Coulomb breakup. The blue band denotes the range of predicted ^{7}Li yields [4]. Observational data are indicated by horizontal green-hatched areas: the upper one has been derived from the recent review of lithium observations by Spite and Spite [5]; the lower one corresponds to the largest ^{6}Li yield reported for the star HD 84937 [13]. The yellow vertical band shows the WMAP η value [1].

VI. PRODUCTION OF ^{6}Li IN THE BIG BANG

The ^{2}H$(\alpha,\gamma)^6$Li reaction is the main path for ^{6}Li BBN production while destruction proceeds via the ^{6}Li(p,α)^{3}He reaction. Both rates are available in the NACRE [43] compilation. While the latter reaction rate is reasonably well known at BBN energies, prior to this experiment the former suffered from a large uncertainty. This was mainly due to the fact that the published error margins were aimed at including the Kiener *et al.* [21] measurement [44]. As a result from the present study, we can now propose a more reliable central value based on a successful theoretical model, and a safe upper limit that is even somewhat smaller than the previous NACRE upper limit.

In Fig. 11, the BBN abundances of ^{7}Li and ^{6}Li are displayed as a function of the baryonic density. (It is usual to introduce another parameter η, the ratio of the number of baryons over the number of photons which remains constant during the expansion, and which is directly related to Ω_b by $\Omega_b = 3.65 \times 10^7 \eta$.) The blue ^{7}Li band is the result of a Monte Carlo calculation taking into account nuclear uncertainties as described in Ref. [4]. The upper hatched horizontal area in the figure shows the primordial lithium (^{6}Li + ^{7}Li) abundance derived from the "Spite plateau," i.e., from the practically metallicity-independent Li observations in metal-poor stars [5].

The solid red line for ^{6}Li has been calculated within the same physical model, using the theoretical reaction rate from this work for ^{2}H$(\alpha,\gamma)^6$Li. Both $E1$ and $E2$ contributions have been included. At WMAP baryonic density, a value for the ^{6}Li/H production ratio of $\approx 1.3 \times 10^{-14}$ results. The dashed red line represents a very conservative upper limit for ^{2}H$(\alpha,\gamma)^6$Li that would hold if the low-energy S_{24} data points from this work resulted from CD only. Figure 7 demonstrates clearly that this is not the case. But even this extremely conservative limit is about two orders of magnitude smaller than the only positive observation of ^{6}Li surviving after the reanalysis of Li lines by Steffen *et al.* [13], indicated in Fig. 11 by the lower hatched horizontal band. This finding corroborates earlier statements (e.g., [4,5]) that observations—if confirmed—of ^{6}Li primordial yields around

TABLE II. Recommended ^{2}H(α,γ)^{6}Li reaction rates using theoretical $E1$ and $E2$ S factors from the present work for the temperature range 10^6 K $\leqslant T \leqslant 10^{10}$ K ($10^{-3} \leqslant T_9 \leqslant 10$).

T_9	$N_a\langle\sigma v\rangle$ (cm^3 mol^{-1} s^{-1})	T_9	$N_a\langle\sigma v\rangle$ (cm^3 mol^{-1} s^{-1})
0.001	0.9153×10^{-29}	0.140	0.6967×10^{-04}
0.002	0.2610×10^{-22}	0.150	0.9495×10^{-04}
0.003	0.3458×10^{-19}	0.160	0.1261×10^{-03}
0.004	0.3190×10^{-17}	0.180	0.2090×10^{-03}
0.005	0.7929×10^{-16}	0.200	0.3237×10^{-03}
0.006	0.9163×10^{-15}	0.250	0.7846×10^{-03}
0.007	0.7672×10^{-14}	0.300	0.1557×10^{-02}
0.008	0.4990×10^{-13}	0.350	0.2715×10^{-02}
0.009	0.2100×10^{-12}	0.400	0.4325×10^{-02}
0.010	0.6547×10^{-12}	0.450	0.6453×10^{-02}
0.011	0.1655×10^{-11}	0.500	0.9169×10^{-02}
0.012	0.3612×10^{-11}	0.600	0.1674×10^{-01}
0.013	0.7142×10^{-11}	0.700	0.2813×10^{-01}
0.014	0.1325×10^{-10}	0.800	0.4502×10^{-01}
0.015	0.2363×10^{-10}	0.900	0.6944×10^{-01}
0.016	0.4103×10^{-10}	1.000	$0.1033 \times 10^{+00}$
0.018	0.1157×10^{-09}	1.250	$0.2359 \times 10^{+00}$
0.020	0.2965×10^{-09}	1.500	$0.4350 \times 10^{+00}$
0.025	0.2014×10^{-08}	1.750	$0.6839 \times 10^{+00}$
0.030	0.8452×10^{-08}	2.000	$0.9623 \times 10^{+00}$
0.040	0.6594×10^{-07}	2.500	$0.1549 \times 10^{+01}$
0.050	0.2827×10^{-06}	3.000	$0.2132 \times 10^{+01}$
0.060	0.8598×10^{-06}	3.500	$0.2705 \times 10^{+01}$
0.070	0.2094×10^{-05}	4.000	$0.3280 \times 10^{+01}$
0.080	0.4372×10^{-05}	5.000	$0.4476 \times 10^{+01}$
0.090	0.8156×10^{-05}	6.000	$0.5754 \times 10^{+01}$
0.100	0.1397×10^{-04}	7.000	$0.7088 \times 10^{+01}$
0.110	0.2240×10^{-04}	8.000	$0.8438 \times 10^{+01}$
0.120	0.3406×10^{-04}	9.000	$0.9773 \times 10^{+01}$
0.130	0.4959×10^{-04}	10.00	$0.1107 \times 10^{+02}$

a few percent of the Spite plateau would require astrophysical sources other than BBN.

In order to facilitate astrophysical calculations of stellar ^{6}Li synthesis with our new theoretical $E1$ and $E2$ S factors, we list in Table II the reaction rates for the temperature range 10^6 K $\leqslant T \leqslant 10^{10}$ K.

VII. CONCLUSIONS

A kinematically complete measurement of the high-energy breakup of ^{6}Li at 150 A MeV has shown that Coulomb and nuclear contributions and their interferences have to be taken into account when interpreting the measured angular distributions. Although it was not possible to extract the Coulomb part experimentally, we were able to infer the $E2$ component of the astrophysical S_{24} factor for the ^{2}H(α,γ)^{6}Li reaction from a theoretical reaction model that describes well in particular the low-energy breakup data. The model predicts a drop of S_{24} with decreasing relative ^{2}H-α energy, $E_{\rm rel}$, as predicted also by most other nuclear models for ^{6}Li, contrary to conclusions from an earlier CD experiment performed at the lower energy of 26 A MeV. We have presented evidence that this earlier experiment probably measured mostly nuclear breakup of ^{6}Li. Our findings allow us to make new predictions for the ^{6}Li/H production ratio in Big Bang nucleosynthesis that is orders of magnitudes smaller than the one derived from claimed observations of ^{6}Li in old metal-poor stars. Sources other than BBN have therefore to be invoked for ^{6}Li production if those observations are confirmed.

ACKNOWLEDGMENTS

We thank N. Kurz for his tireless help with the data acquisition. Thanks go to P. Descouvemont and K. Nollett for kindly providing numerical results from their theoretical calculations. This research was supported by the DFG Cluster of Excellence "Origin and Structure of the Universe."

[1] WMAP Collaboration, E. Komatsu *et al.*, arXiv:1001.4538, Astrophys. J. Suppl. Ser. **5** (to be published).
[2] A. Coc, E. Vangioni-Flam, P. Descouvemont, A. Adahchour, and C. Angulo, Astrophys. J. **600**, 544 (2004).
[3] R. H. Cyburt, B. O. Fulop, and K. A. Olive, J. Cosmol. Astropart. Phys. 11 (2008) 012.
[4] A. Coc and E. Vangioni, in *Proceedings of the Fourth International Conference on Nuclear Physics and Astrophysics* [J. Phys. Conf. Ser. **202**, 012001 (2010)].
[5] M. Spite and F. Spite, in *Light Elements in the Universe, Proceedings of the IAU Symposium No. 268, 2010*, arXiv:1002.1004.
[6] M. Asplund, D. Lambert, P. E. Nissen, F. Primas, and V. Smith, Astrophys. J. **644**, 229 (2006).
[7] E. Rollinde, E. Vangioni, and K. A. Olive, Astrophys. J. **651**, 658 (2006).
[8] V. Tatischeff and J. P. Thibaud, Astron. Astrophys. **469**, 265 (2007).
[9] M. Kusakabe, T. Kajino, R. N. Boyd, T. Yoshida, and G. J. Matthews, Astrophys. J. **680**, 846 (2008).
[10] J. Ellis, K. A. Olive, and E. Vangioni, Phys. Lett. B **619**, 30 (2005).
[11] K. Jedamzik, Phys. Rev. D **74**, 103509 (2006).
[12] R. Cayrel *et al.*, Astron. Astrophys. **473**, L37 (2007); in *Proceedings of the Tenth Symposium on Nuclei in the Cosmos, Mackinac Island, Michigan, 2008*, arXiv:0810.4290.
[13] M. Steffen, R. Cayrel, P. Bonifacio, H.-G. Ludwig, and E. Caffau, in *Light Elements in the Universe* (Ref. [5]), arXiv:1001.3274.
[14] A. E. Garcia Perez, W. Aoki, S. Inoue, S. G. Ryan, T. K. Suzuki, and M. Chiba, Astron. Astrophys. **504**, 213 (2009).
[15] M. Asplund and K. Lind, in *Light Elements in the Universe* (Ref. [5]), arXiv:1002.1993.
[16] P. D. Serpico, S. Esposito, F. Iocco, G. Mangano, G. Miele, and O. Pisanti, J. Cosmol. Astropart. Phys. 12 (2004) 010.
[17] R. G. H. Robertson, P. Dyer, R. A. Warner, R. C. Melin, T. J. Bowles, A. B. McDonald, G. C. Ball, W. G. Davies, and E. D. Earle, Phys. Rev. Lett. **47**, 1867 (1981).
[18] P. Mohr, V. Kölle, S. Wilmes, U. Atzrott, G. Staudt, J. W. Hammer, H. Krauss, and H. Oberhummer, Phys. Rev. C **50**, 1543 (1994).
[19] F. E. Cecil, J. Yan, and C. S. Galovich, Phys. Rev. C **53**, 1967 (1996).

[20] G. Baur, C. A. Bertulani, and H. Rebel, Nucl. Phys. A **458**, 188 (1986).
[21] J. Kiener, H. J. Gils, H. Rebel, S. Zagromski, G. Gsottschneider, N. Heide, H. Jelitto, J. Wentz, and G. Baur, Phys. Rev. C **44**, 2195 (1991).
[22] R. Shyam, G. Baur, and P. Banerjee, Phys. Rev. C **44**, 915 (1991).
[23] S. B. Igamov and R. Yarmukhamedov, Nucl. Phys. A **673**, 509 (2000).
[24] A. Kharbach and P. Descouvemont, Phys. Rev. C **58**, 1066 (1998).
[25] B. Jenny, W. Grüebler, V. König, P. A. Schmelzbach, and C. Schweizer, Nucl. Phys. A **397**, 61 (1983).
[26] L. C. McIntyre and W. Haeberli, Nucl. Phys. A **91**, 382 (1967).
[27] W. Grüebler, P. A. Schmelzbach, V. König, P. Risler, and D. Boerma, Nucl. Phys. A **242**, 265 (1975).
[28] S. Typel, H. H. Wolter, and G. Baur, Nucl. Phys. A **613**, 147 (1997).
[29] A. C. Betker, C. A. Gagliardi, D. R. Semon, R. E. Tribble, H. M. Xu, and A. F. Zaruba, Phys. Rev. C **48**, 2085 (1993).
[30] H. Okamura *et al.*, Phys. Rev. C **58**, 2180 (1998).
[31] B. Bonin *et al.*, Nucl. Phys. A **445**, 381 (1985).
[32] K. Schwarz *et al.*, Eur. Phys. J. A **7**, 367 (2000).
[33] E. D. Cooper, S. Hama, B. C. Clark, and R. L. Mercer, Phys. Rev. C **47**, 297 (1993).
[34] E. Bauge, J. P. Delaroche, and M. Girod, Phys. Rev. C **58**, 1118 (1998).
[35] H. Geissel *et al.*, Nucl. Instrum. Methods Phys. Res., Sect. B **70**, 286 (1992).
[36] P. Senger *et al.*, Nucl. Instrum. Methods Phys. Res., Sect. A **327**, 393 (1993).
[37] N. Iwasa *et al.*, Phys. Rev. Lett. **83**, 2910 (1999); F. Schümann *et al.*, Phys. Rev. C **73**, 015806 (2006).
[38] GEANT Detector Description and Simulation Tool, CERN Program Library Long Writeup W5013, 1993.
[39] K. Langanke, Nucl. Phys. A **457**, 351 (1986).
[40] K. M. Nollett, R. B. Wiringa, and R. Schiavilla, Phys. Rev. C **63**, 024003 (2001).
[41] A. M. Mukhamedzhanov, R. P. Schmitt, R. E. Tribble, and A. Sattarov, Phys. Rev. C **52**, 3483 (1995).
[42] L. D. Blokhintsev, S. B. Igamov, M. M. Nishinov, and R. Yarmukhamedov, Yad. Fiz. **69**, 456 (2006) [Phys. At. Nucl. **69**, 433 (2006)].
[43] NACRE Compilation, C. Angulo *et al.*, Nucl. Phys. A **656**, 3 (1999).
[44] C. Angulo (private communication).